Helical to Ring Transition in Coassembled Cylindrical Micelles Formed from Charged Peptide Amphiphiles

Undergraduate Researcher
Marc Michael D. Lim
Northwestern University

Faculty Mentor
Monica Olvera de la Cruz
Department of Materials Science and
Engineering, Northwestern University

Postdoctoral Mentors
Graziano Vernizzi
Department of Materials Science and
Engineering, Northwestern University

Yury S. Velichko
Department of Materials Science and
Engineering, Northwestern University

Abstract

Surface patterns, formed by the coassembly of cationic-anionic amphiphiles into cylindrical micelles, were analyzed. The competition between electrostatic forces and the net incompatibility χ arising from the different chemical natures of those oppositely charged amphiphiles resulted in the formation of segregated domains. These surface domains are not macroscopically segregated due to the electrostatics penalty associated with their growth. In charged stoichiometric coassemblies into cylinders, a lamellar-charged surface pattern is predicted analytically and observed by Monte Carlo simulations. The symmetry of the lamellar pattern is either ring (perpendicular to the long cylinder axis) or helical. Previous work was extended by incorporating variance of the dielectric constant of the medium ε_o to different values of the cylinder's radius R_c and χ and studying how the transition between these two symmetries is affected. The critical surface in the space $\{R_c, \varepsilon_o, \chi\}$ separating the helical and ring symmetries is presented and its dependence on ε_o computed. It was found that ε_o is a significant parameter in the control of the helical-ring transition; the

ring pattern is strongly associated with the prevalence of short-range nonelectrostatic forces, while the helical pattern develops in response to a greater predominance of long-range electrostatic strain.

Introduction

Self-aggregating peptide amphiphiles (PAs) can be designed to form cylindrical micelles that in turn can mimic the extracellular matrix and thus cell support; in order to promote the growth of specific tissues within these micelles, epitopes can be added to the fibers.[1] PAs are composed of a hydrophobic block connected to a peptide block that favors β-sheet formation. The peptides are selected such that the head groups are polar, which, upon aggregation, preferentially expose themselves at the surface and thus interact at the water interface. Electrostatic repulsion makes the assembly of single-component charged amphiphilic molecules highly unfavorable.[2,3] Thus, peptide blocks must be neutral (high pH for acidic PAs and low pH for basic PAs) or salt concentration must be extremely high so that single-component PAs assemble. However, at physiological pH conditions, stoichiometric mixtures of acidic (-) and basic (+) PAs that carry net charge have been shown to coassemble at 1% wt into nanofibers with a diameter of about 6–8 nm.[4] As noted earlier, the polar head groups make up the surface of these fibers; by specifically selecting their amino acids sequences, these nanofibers can be designed to promote the growth of bone,[5] or neural cell differentiation.[6]

This study analyzed immiscible species of amphiphilic molecules — cationic and anionic — coassembled into a cylindrical micelle. Because the electrostatic

attraction and immiscibility of these molecules counteracted each other, internal energy was minimized through the adoption of distinct surface patterns composed of dispersed aggregates of the two species. Charged surface heterogeneities resulted in surface patterns of various symmetries, including isotropic, locally correlated, zigzag, helical, and ring. Additionally, there were transitional symmetries with defects.[7] The specific pattern that occurs can be directed through the varying of a number of parameters. In this particular study, the transition between the lamellar and ring pattern was studied and characterized as a function of the cylindrical radius R_c, the dielectric constant ε_o, and the net degree of compatibility χ.

Background

Electrostatics plays a key role in biomolecular assembly. For example under appropriate ionic conditions, oppositely charged biomolecules (e.g., those of actin-binding protein complexes and DNA and histone proteins) will coassemble into functional units like cytoskeleton components and nucleosomes. When electrostatics are balanced with packing limitations, such coassemblies often develop surface-charge heterogeneities which in turn affect the interactions with charged surfaces or similar aggregates. Oftentimes, this involves symmetry breaking, which then affects functional abilities and structural changes. These in turn influence the order of coassemblies, which makes the determination of the physical characteristics of these surface-charged heterogeneities of particular interest. Biomolecules that have hydrophobic groups have assemblies whose structure is influenced by both the fundamental shape of the molecules as

well as the intermolecular interactions of the components. The coassemblies of these biomolecules can have symmetries that are spherical, cylindrical, or planar in nature. Oppositely charged lipids for example, coassemble into cylindrical micelles[8] or into vesicles,[9] while mixtures of cationic and anionic peptide amphiphiles capable of β-sheet formation coassemble into rigid cylindrical micelles due to hydrogen bonds, hereafter referred to as fibers.[4,6] Surface properties, which result from competing interactions, in turn influence the stability of these assemblies.[10] Coassemblies with competing interactions lead to surfaces

with charge heterogeneities. Here we analyze the surface patterns on cylindrical coassemblies.

In cationic-anionic coassemblies there are several factors that contribute to the forming of surface heterogeneities. The net incompatibility among chemically different charged components, which in water can be due to different degrees of hydrophobicity, promotes macroscopic segregation of the different components. Meanwhile, electrostatics favors correlated ionic crystal structures. The competition of these interactions results in the formation of surface charge patterns[7,11,12] in aqueous interfaces due to the high permittivity of the water. In

dense media, charges are paired, while in water they can be dissociated. At the interface between a dense medium and an aqueous solution, charged patterns of different length scales are possible because the mean permittivity of the two media is sufficiently high. The formation of large domains that decrease the interface among the components is restricted due to the penalty associated with charge accumulation. The resulting surface patterns in stochiometric 1:1 charged systems are lamellar structures of periodicity determined by the effective or net permittivity of the media at the aqueous interface and net incompatibility among the components. When the amphiphiles are restricted to cylindrical
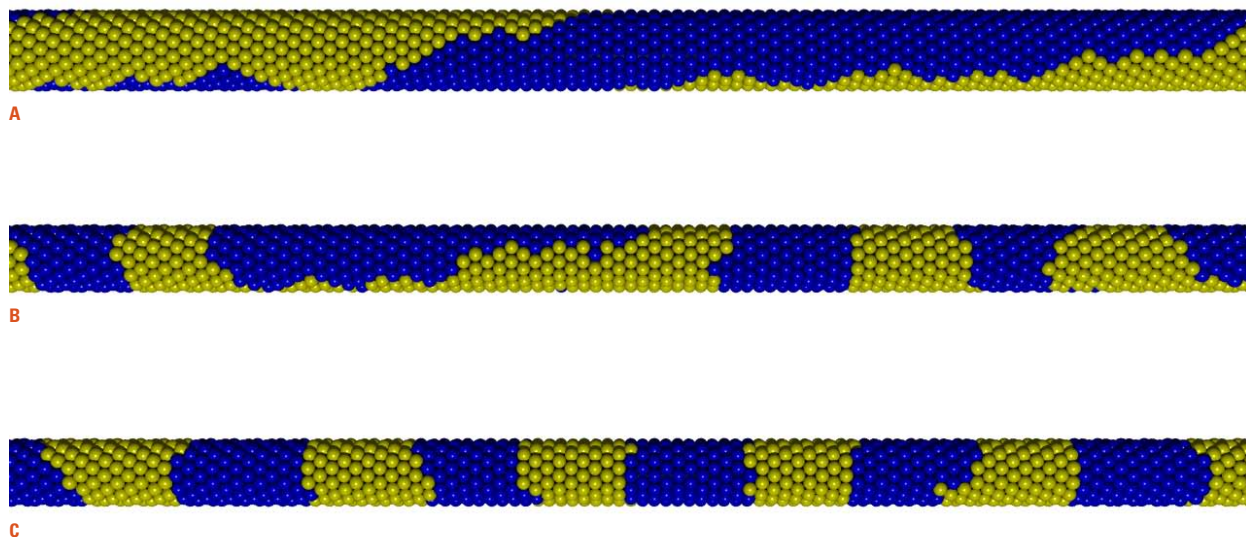
A

B

C

Figure 1: Typical configurations for (A) the helical symmetry ($\chi = 12$, Rc = 2.5, $\varepsilon_0 = 30$); (B) the transitional symmetry ($\chi = 8.5$, Rc = 2, $\varepsilon_0 = 30$); and (C) the ring symmetry ($\chi = 10$, Rc = 2, $\varepsilon_0 = 25$). Note the coexistence of both the helical and ring symmetries in (B).

micelles, the lamellar pattern can have various symmetries, including the ring and helical structures analyzed here.

Approach

Metropolis Monte Carlo simulations were employed to determine the surface patterns on coassembled cationic-anionic cylindrical micelles. A lattice fluid consisting of two species, one of which is positive and the other of which is negative with equal absolute charge $|Q_+|$ = $|Q_-|$ and occurring in equal ratios, was confined to a cylindrical monolayer of radius Rc and length $L_C = L_Z$. This in turn was placed in the center of the box L x L x L_Z so that the long axis was parallel

to the z axis. These units were modeled as spheres of diameter σ = 1 and were arranged on the surface of the cylinder in such a way that all units occurred in the knots of a triangular lattice of period $a = \sigma$ (Figure 1). Cylindrical geometry is rigid and molecules are only allowed to move about the surface (that is, they cannot go into solution) due to the consideration of each aggregate as a stable structure.

The net degree of compatibility in k_BT units is defined as

$$\chi = n[\eta_{+-} - (\eta_{--} + \eta_{++})/2]$$

where $n = 6$ is the number of nearest

neighbors in the lattice. In this simulation, $\chi = -3\eta_{++}$, because we only have short-range nonelectrostatic attraction among positively charged molecules. This is correct because the system is incompressible — there are no vacancies or neutral molecules; in a compressible model all the interactions would have to be included. χ describes the effective nonelectrostatic interaction among the coassembled macromolecules and not among individual head groups. Therefore, this parameter can be much larger than one for real systems. Moreover, in the systems with only Van der Waals interactions, χ is proportional to $1/T$; however, in systems with hydrophobic and hydrogen bonding
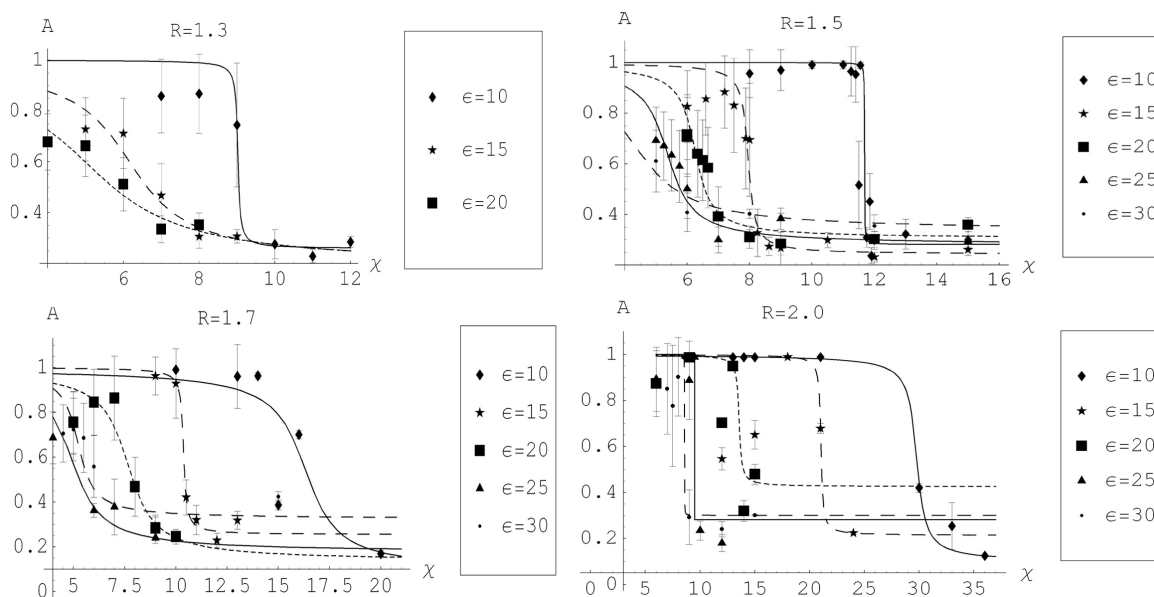

Figure 2: Plots of asphericity A as a function of χ. Note the generally sharp transition between the helical and ring surface patterns.

interactions, such as in coassembled PAs, the interactions may have a complex T dependence. Excluded volume and electrostatic interactions were also considered. This system, which is the same as that used by Velichko and Olvera de la Cruz,[7] has a Hamiltonian that reads as follows:

$$\frac{H}{k_B T} = \sum_{i>j}^{N} \frac{Q_i Q_j}{\varepsilon_o r_{ij}} + \sum_{\{i,j\}}^{N} \frac{\eta_{++}(Q_i + Q_+)(Q_j + Q_+)}{(2Q_+)^2}$$

where Q_i is a charge of the i th unit, ε_o is the average dielectric constant of the media in units

$$e^2 / 4\pi\sigma , \ r_{ij} = \left| \overline{r}_j - \overline{r}_i \right| / \sigma$$

is a dimensionless distance between ith and jth units, $\mathbf{r}_i$ determines the position of the ith unit in the space $Q_+ = 1$, and the summation in the second term is only over nearest neighbors. To exclude interaction with displaced image-cylinders, periodical boundary conditions are applied only in the z direction and, thus, Lekner summation technique[13] is used to calculate the electrostatic energy of the single cylinder system

$$\frac{E_{el}}{k_B T} = \frac{1}{2\varepsilon_o} \sum_{i,j=0}^{N} \sum_{m=-\infty}^{\infty} \frac{Q_i Q_j}{\sqrt{\rho_{ij}^2 + (z_{ij} + mL_z)^2}}$$

where

$$\rho_{ij} = \left(x_{ij}^2 + y_{ij}^2 \right)^{1/2}$$

and for $m = 0$ the terms with $i = j$ are omitted. Standard canonical Monte Carlo simulations following the Metropolis scheme for various values of $\varepsilon_{++} \in [-5,-1]$, $\varepsilon_o \in [10,30]$, $R_c \in [1,3,2]$

and $L_c / \sigma = 100$ are reported. Simple moves in the pattern space were performed by the exchange of two randomly chosen particles. Each system is equilibrated during either 10^3 or 5 x 10^3 MC steps per particle, and another 5 x 10^3 MC steps were used to perform measurements. The equilibration process was accompanied by a gradual decrease of temperature (temperature annealing) from $T_{\max}$ to $T_{\min}$ (in units with $k_B = 1$).

Results

The simulation yielded configurations that were either helical, ring, or transitional in character. In order to find χ^*, the exact value of χ at which the transition between the helical and ring phase for a given R_c and ε_o occurs, the asphericity A(C), a parameter introduced by Rudnik and Gaspar that characterizes the anisotropy of the system,[14] was calculated for each Monte Carlo configuration according to the equation

$$A = \frac{\left\langle (Tr[T])^2 - 3M[T] \right\rangle}{\left\langle (Tr[T])^2 \right\rangle}$$

In this equation, T is the inertia matrix for each independent cluster C on the cylinder surface defined such that

$$T_{\alpha\beta} = \frac{1}{N_C^2} \sum_{i>j}^{N_C} \left(\mathbf{r}_i - \mathbf{r}_j \right)_\alpha \left(\mathbf{r}_i - \mathbf{r}_j \right)_\beta$$

with N_c equivalent to the number of ions in the cluster and $\mathbf{r}_i{}^\alpha$ the αth Cartesian component of the position vector of the ith ion. Using this output, the ensemble average $<A>$ was simply obtained by

$$<A> = \frac{1}{n} \sum_{i=1}^{n} A(C_i)$$

The error associated to this observable scales like $1 / \sqrt{N}$, where N is the number of independent Monte Carlo samplings. It is well known that N is not usually equal to n, since the configurations generated by any Monte Carlo algorithm are typically correlated. To correct for this, one can compute the autocorrelation length τ of the sequence $\{A(C_i)\}$ and then subsample the same set of configurations, keeping one configuration every τ and skipping all the configurations in between. Then the standard deviation of the remaining data is used as a best estimate for the error δA on $<A>$.

In Figure 2 plots of the asphericity $<A>$ as a function of χ are shown (at fixed R_c and ε_o). The general behavior is that at low values of χ, the helical phase dominates and the asphericity is close to its maximum value 1, whereas at larger values of χ, the ring phase starts and the asphericity decreases towards zero. Each plot was interpolated with a standard sigmoid function

$$A(\chi) = \alpha_1 + \alpha_2 \ \tanh(\gamma (\chi - \chi^*)$$

with parameters α_1, α_2 and γ that control the asymptotes at large χ, the slope at the transition point χ^*, and the transition point χ^* itself. The interpolation of the data points has been done by using the weighted least-square minimization method, i.e., by minimizing the function

$$G(\alpha_1, \alpha_2, \gamma) = \sum_i \left(\frac{A(\chi_i) - A_i}{\delta A_i} \right)^2$$

This method finds the value of the transition point χ^* and its error $\delta\chi^*$ (by the error propagation method) very
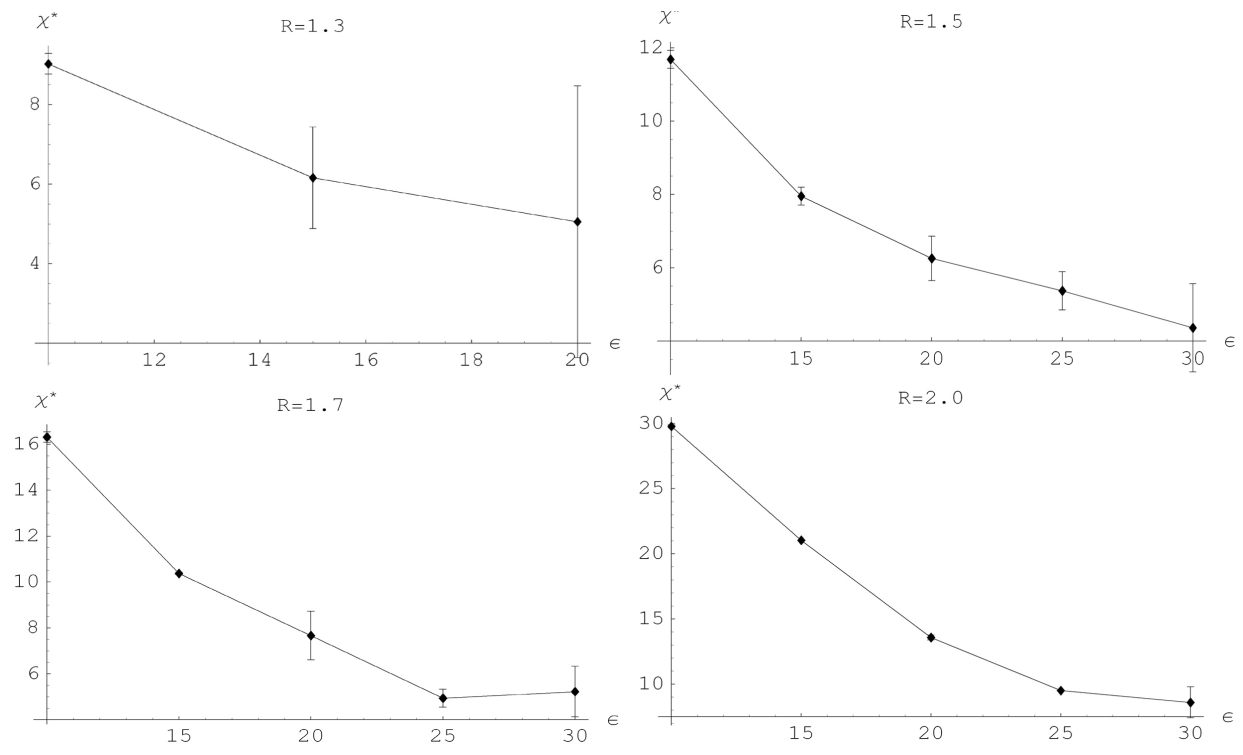
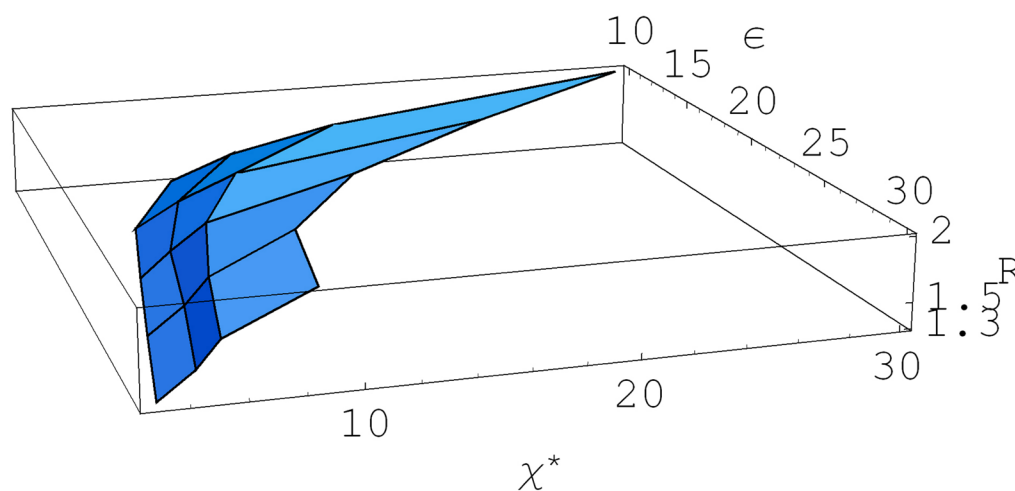**Figure 3:** χ^* **and its errors are plotted as a function of** ϵ_0 **for all values of Rc.**

Figure 4: Three-dimensional rendering of the critical surface separating the ring phase from the helical phase in the configuration space {R, εo, χ}.

efficiently. All the numerical minimizations and the preparation of the plots were done by using the Mathematica 5.2 software by Wolfram Research.

In Figure 3 values of χ^* and its errors are plotted as a function of ε_o for all values of R_c. In Figure 4 all of these plots are combined into a three-dimensional diagram so as to give a complete overview of the critical surface separating the ring phase from the helical phase in the configuration space $\{R_c, \varepsilon_o, \chi\}$.

Discussion

These data show that systems highly influenced by electrostatic forces tend to favor the helical state, while those systems that are more strongly governed by short-range, nonelectrostatic interactions have a tendency towards the ring symmetry. The helical symmetry allows for electrostatic reactions through the center of the cylinder to be minimized. Therefore, one expects that this symmetry will be preferentially observed when electrostatics dominate. On the other hand, when electrostatics do not exist, the system will be macroscopically segregated, with half of the cylinder being of one type and the other being the other half (an infinite ring phase). Therefore, it is expected that as one begins to introduce electrostatic interactions, this ring symmetry will be preferred due to its minimization of the interfacial energy between the two components.

For fixed ε_o, we find that χ^* from helical to ring increases as R_c increases. This is due to the reasons discussed above — as χ increases, nonelectrostatic forces that favor macroscopic segregation become more prominent. The ring symmetry greatly decreases the total interface length between the two species; that is,

it promotes more net aggregation. With increasing R_c, there are more charged molecules present; the gain in electrostatic forces due to the increased volume of charges requires a higher χ to be overcome.

As with a fixed ε_o, a fixed χ leads to a positive correlation between ε_o and R_c for many of the same reasons. However, rather than promoting nonelectrostatic forces, the dielectric constant hinders the strength of electrostatic interactions, though to much the same effect.

For fixed R_c, it is seen that the helical symmetry exists only when one or both of the variables χ and ε_o are low. The relation with low χ is rather apparent; as explained above, χ promotes the development of the ring phase. With ε_o, one must be aware that it serves as a screen for charge; the higher the value of ε_o, the greater the amount of screening

and thus the less influence exerted by electrostatics. Thus, when ε_o is low, even for very high values of χ (>10), the helical phase persists.

Conclusions

From this work, it can be seen that the default symmetry for high electrostatic influence is helical — that is, it is favored when ε_o and χ are low or R_c is high. The ring symmetry is favored where short-range, nonelectrostatic forces are dominant — either when those forces are high due to a large χ, or when electrostatics are weakened due to a large ε_o or low R_c. These results could be used to design cationic-anionic micelles with specific interactions and radii for helical lamellar structures. These structures can change the conductivity of fibers if metal ions are adsorbed on the surfaces of the fiber; for instance, it is believed that the ring structure will be an insulator. Applications of these ideas may be of interest for technological applications.

Note that although this program was developed and executed with relevance to peptide amphiphiles in mind, it is applicable to other systems such as micelles of coassembled cationic-anionic simple lipids. By ignoring β-sheet formation in peptide amphiphiles, the possibility of far more complex interactions and surface patterns remains open. The interactions in peptides are not isotropic in space and favor stronger effective repulsion between opposite charges along the β-sheet axis, which is most probably the z axis of the cylinder. Therefore, the lamella may form along the z axis. Future iterations of our model must incorporate such considerations.

Future work also includes analysis of screening length κ effects, which are controlled by the presence of salt ions in solution.

References

(1) Guler, M. O.; Hsu, L.; Soukasene, S.; Harrington, D. A.; Hulvat, J. F.; Stupp, S. I. *Biomacromolecules* **2006,** *7,* 1855–1863.

(2) Huang, C.; Olvera de la Cruz, M.; Delsanti, M.; and Guenoun, P. *Macromolecules* **1997,** *30,* 8019.

(3) Borisov, O. V. and Zhulina, E. B. *Macromolecules* **2003,** *36,* 10029.

(4) Niece, K. L.; Hartgerink, J. D.; Donners, J. J.; Stupp, S. I. *J. Am. Chem. Soc.* **2003,** *125,* 7146–7147.

(5) Hartgerink, J. D.; Beniash, E.; and Stupp, S. I. *Science* **2001,** *294,* 1684.

(6) Silva, G. A.; Czeisler, C.; Niece, K. L.; Beniash, E.; Harrington, D.A.; Kessler, J. A.; and Stupp, S. I. *Science* **2004,** *303,* 1352–1355.

(7) Velichko, Y. S. and Olvera de la Cruz, M. *Phys. Rev. E* **2005,** *72,* 041920.

(8) Kaler, E. W.; Herrington, K. L.; Murthy, A. K.; and Zasadzinski, J.A. N. *J. Phys. Chem.* **1992,** *96,* 6698.

(9) Dubois, M.; Deme, B.; Gulik-Krzywicki, T.; Debieu, J. C.; Vautrin, C.; Perez, E.; and Zemb, T. *Nature* **2001,** *411,* 672.

(10) Gitlin, I.; Carbeck, J. D.; and Whitesides, G. M. *Angew. Chem. Intern. Ed.* **2006,** *45,* 3022–3060.

(11) Meyer, E. E.; Lin, Q.; Hassenkam, T.; Oroudjev, E.; and Israelachvili, J. N. *PNAS* **2005,** *102,* 6839.

(12) Solis, F. J.; Stupp, S. I.; and Olvera de la Cruz, M. *J. Chem. Phys.* **2005,** *122,* 054905.

(13) Grzybowski, A. and Bródka, A. *Mol. Phys.* **2002,** *100,* 625.

(14) Rudnick, J. and Gaspari, G. *J. Phys. A* **1986,** *19,* L191.